Quantification of Spatial Pharmacogene Expression Heterogeneity in Breast Tumors

Nicholas R Powell
Indiana University School of Medicine https://orcid.org/0000-0003-4572-0733
Rebecca M Silvola
Indiana University School of Medicine
John S Howard
Indiana University School of Medicine
Sunil Badve
Emory University School of Medicine
Todd C Skaar
Indiana University School of Medicine
Joseph Ipe (joseph.ipe@10xgenomics.com)
Indiana University School of Medicine

Research article

Keywords: spatial, transcriptomics, pharmacogene, chemotherapy, resistance

Posted Date: November 22nd, 2021

DOI: https://doi.org/10.21203/rs.3.rs-1043506/v1

Abstract

Background: Chemotherapeutic drug concentrations vary across different regions of tumors and this is thought to be involved in development of chemotherapy resistance. Insufficient drug delivery to some regions of the tumor may be due to spatial differences in expression of genes involved in the disposition, transport, and detoxification of drugs (pharmacogenes). Therefore, in this study, we analyzed the spatial expression of 286 pharmacogenes in 6 breast cancer tissues using the recently developed Visium spatial transcriptomics platform to (1) determine if these pharmacogenes are expressed heterogeneously across tumor tissue and (2) to determine which pharmacogenes have the most spatial expression heterogeneity.

Methods: The spatial transcriptomics technology sequences the transcriptome of 55 um diameter barcoded sections (spots) across a tissue sample. We analyzed spatial gene expression profiles of four biobank-sourced breast tumor samples in addition to two breast tumor sample datasets from 10X genomics.

Results: Collectively, we identified 8887 spots in tumor regions, 3814 in stroma, 44 in lymphocytes, and 116 in normal regions based on pathologist annotation of the tissues. We showed statistically significant differences in expression of pharmacogenes in tumor regions compared to surrounding non-tumor regions. We also observed that the most heterogeneously expressed genes within tumor regions were involved in ROS handling and detoxification mechanisms. GPX4, GSTP1, MGST3, SOD1, CYP4Z1, CYB5R3, GSTK1, and NAT1 showed the most heterogeneous expression within tumor regions.

Conclusions: The heterogeneous expression of these pharmacogenes may have important implications for cancer therapy due to their ability to impact drug distribution and efficacy throughout the tumor. Notably, our results suggest that chemoresistance caused by expression of GPX4, GSTP1, MGST3, and SOD1 may be intrinsic, not acquired, since the heterogeneity is not specific to chemotherapy-treated samples or cell type.

Background

Heterogeneity is one of the hallmarks of cancer (1) and is associated with resistance to treatment, poor prognosis, and treatment failure (2–4). Intratumor heterogeneity exists at multiple levels including genetic, epigenetic, metabolic, and transcriptional (5–10). Spatial transcriptomic changes can lead to phenotypic variability in traits such as cellular morphology (11), growth (12), metabolism (13), immune function (14), angiogenicity (15), reactive oxygen handling (16, 17), and solute transport (18). These phenotypic changes that result from transcriptionally distinct regions of the tumor are subsequently able to confer resistance to anti-cancer therapies (19).

Success of systemic anti-cancer therapy is dependent upon the ability to deliver cytotoxic concentrations of the drug to all cells within a tumor. Drug concentrations vary across different regions of tumors (20) and is thought to be involved in development of resistance (21). Insufficient drug delivery to some regions of the tumor may be due to spatial differences in expression of genes involved in the disposition and

transport of drugs (pharmacogenes). Drug transporters such as the solute-carrier protein (SLC) and the ATP-binding cassette (ABC) family are membrane proteins that transport a wide variety of molecules, including anti-cancer agents, and have been linked with multidrug resistance in cancers (22, 23). This mechanism of resistance is thought to involve survival of certain tumor cells with strong drug efflux mechanisms (24–27), which seed resistant cancer cells that clonally expand and regenerate the tumor after chemotherapy treatment (28).

Transporters are not the only mechanism of chemotherapeutic resistance. Several chemotherapeutic agents alter the redox homeostasis of cancer cells by elevating levels of reactive oxygen species (ROS) and inducing ROS mediated cell injury (29, 30). Aberrant expression of ROS handling enzymes, including detoxifying enzymes such as superoxide dismutase (SOD) (31) and glutathione peroxidase (GPX) (32) can also promote development of regions across the tumors that are resistant to anti-cancer agents.

Spatial expression of other pharmacogenes involved in the pharmacokinetics (PK) of chemotherapeutic agents, like the CYP450 enzymes, could also be involved in spatial differences in tumor drug concentrations. Therefore, in this study, we analyzed the spatial expression of 286 pharmacogenes in 6 breast cancer tissues using the recently developed Visium spatial transcriptomics platform (33) to determine if these pharmacogenes are expressed heterogeneously across tumors and to determine which pharmacogenes have the most spatial expression heterogeneity.

Methods

Tissue collection

Tissues were obtained from the Indiana Biobank under the approved IRB protocol (number 1803676586) at Indiana University. Consent for research and publication of de-identified research information was provided by subjects of the Indiana Biobank. Surgically resected breast tumors were weighed and divided into ~150 mg tissue chunks that were flash frozen in liquid nitrogen and placed in a cryovial. The tissues were bio-banked and stored in liquid phase of nitrogen until experimental use.

Cryosectioning

A cryomold was placed in an ethanol-dry ice slurry. Tissue was transferred from the cryovial on dry ice to the cryomold using pre-cooled forceps. Pre-cooled optimum cutting temperature (OCT) was added to the cryomold, completely covering the tissue, and allowed to freeze for ~2 minutes. The frozen tissue block was removed and placed on a cryotome chuck using OCT and immediately transferred to a pre-chilled cryotome chamber (Leica CM3050 S). Once frozen, the cryotome chuck was placed on the stage and the tissues were cryosectioned at a thickness of 14-16 µm. The chamber temperature was maintained at -20°C and the specimen head was maintained at -28 to -32°C. Tissue sections were placed within the frames of a pre-chilled Visium Spatial slide. The slide was transferred to a prechilled slide box and stored on dry ice.

Visium Spatial Tissue Optimization and Library Preparation

Visium Spatial Tissue Optimization was done as per manufacturer's instructions using a breast tumor tissue sample sectioned at 16 µm. Based on the tissue optimization, 12 minutes was determined to be the optimal permeabilization time. Imaging was done using a Keyence BZ-X microscope. Visium Spatial library preparation was done as per manufacturer's instructions. H&E-stained tissue images were captured at 10X magnification. Imaging time was 14 minutes per slide. cDNA and library preparation were done at the Center for Medical Genomics core at Indiana University.

Sequencing and Analysis

300 pM dual-indexed libraries were sequenced using Novaseq 6000 and a SP flow cell at 200 cycles per lane. Sample demultiplexing, image alignment, barcode processing, and gene counting was done using the Space Ranger pipeline (10X Genomics). Briefly, spaceranger mkfastq was used to wrap Illumina's bcl2fastq to demultiplex Visium-prepared sequencing runs and to convert barcode and read data to FASTQ files. Spaceranger count was then used to combine the FASTQ file and optical H&E stained tissue image, generate feature-spot matrices, determine clusters, and perform initial gene expression analysis. A Loupe Browser file was created for an interactive visualization functionality.

Data analysis

Broad descriptions of the data analysis are given here, and the scripts used to analyze the data are provided in the supplement. We used R (version 3.6.0) for all analyses. First, pathologist annotated cluster assignments (barcode annotation index) were downloaded from the Loupe Browser and read into R along with the full unique molecular identifier (UMI) read count matrix for each sample. Data was either normalized to (divided by) the total reads per spot or kept as is, depending on the analysis. Log transformation was not performed on read counts for certain analyses (as indicated in the results section) to yield a more intuitive interpretation of the data. Log2 transformation was performed for fold-change analysis. For log transformed data, read counts of zero convert to +/- infinity but are shown in the figures as such since these values are indicative of low expression and therefore should not be discarded. Pharmacogenes were filtered based on a list of 298 pharmacogenes as described by www.pharmaadme.org, resulting in 286 pharmacogenes that were present in the read count matrix. The pharmacogene list is based on input from seven major pharmaceutical companies as to which genes perform or regulate drug metabolism or transport. Spots were filtered by sample or by annotation as needed for each analysis. Interquartile range of read counts (75th -25th percentile) was used to measure heterogeneity because it best characterizes the spread (variability) of data without being too heavily influenced by outlier values. Additionally, it allowed better visual representation than standard deviation or coefficient of variation.

GO analysis

We used MGI Batch (http://www.informatics.jax.org/batch/summary) gene ontology (GO) to classify 35 pharmacogenes involved in reactive oxygen species handling ("ROS genes") (Supplementary Table S1). We conducted the GO pathway analysis using the PANTHER web tool (http://pantherdb.org/tools/compareToRefList.jsp) to identify the GO terms that are significantly

overrepresented (Fisher's exact, Bonferroni p-value < 0.05) by the 66 heterogeneously expressed pharmacogenes.

Results

Summary of Tumor Tissues

We analyzed spatial gene expression profiles of four biobank-sourced breast tumor samples in addition to two breast tumor sample datasets from 10X genomics. The patient demographics and disease characteristics of the biobank samples are listed in Supplementary Table S2.

Spatial gene expression patterns were generated from a total of 13,600 spots across the six tissues with 27,542 genes detected. Supplementary Figure S1 shows that pharmacogenes were evenly distributed across the relative expression range (S1A) and that many of the *CYP* and *SLC* genes were generally expressed at lower levels (S1B). Pharmacogenes involved in ROS handling (ROS genes) and the ABC transporters are generally seen towards the top half of relative expression among the pharmacogenes.

A pathologist's annotation (S.B.) of the H&E-stained sections was used to classify spatially barcoded spots within the tissue as tumor, stroma, lymphocytes, normal, or mixed. A visual representation of the observed spatial heterogeneity in the expression of ABC transporters (as an example) within pathologist-annotated tumor regions are shown in Supplementary Figure S2.

Collectively, we identified 8887 spots in tumor regions, 3814 in stroma, 44 in lymphocytes, and 116 in normal regions. The remaining spots, ~5% of the total, were considered mixed regions that were primarily stroma with presence of tumor cells and were not included in the analysis.

Pharmacogene Expression in Tissues

We interrogated the spatial expression of 286 pharmacogenes across six tissue samples. Out of the 286 pharmacogenes, 259 were expressed in at least one sample and 214 were expressed in all six tissues.

The interquartile range of gene expression across spatially barcoded spots was used as a measure of heterogeneous gene expression. We calculated the interquartile range of gene expression across pathologist-annotated tumor spots in two ways; within each sample individually and combined across all tissue samples. 66 genes were found to have an interquartile range greater than zero, specifically in tumor regions, across the 6 samples. Figure 1 shows the expression levels of these genes within tumor spots from all six tissue samples. GPX4, GSTP1, MGST3, SOD1, CYP4Z1, CYB5R3, GSTK1, and NAT1 showed the most heterogeneous expression.

The heterogeneity of pharmacogene expression across just tumor spots within each of the six tissues is shown in Figure 2A. To account for possible variability in global transcriptional activity in each of the tumor spots, the interquartile range of expression was also determined after pharmacogene expression was normalized to total read counts from each spot (Figure 2B). We observe that GPX4, GSTP1, and

SOD1 are heterogeneously expressed across samples, whereas CYP4Z1, GSTM3, and NAT1 were heterogeneously expressed in only some of the tissues. CYB5R3 and ABCC5 were heterogeneously expressed in all but one of the tissue samples.

We show that the expression of pharmacogenes is also heterogeneous in tumor-associated stroma, lymphocytes, and adjacent normal regions. The interquartile range of pharmacogene expression (Figure 2C and 2D) in these regions demonstrates presence of heterogeneous gene expression in both tumor and tumor-associated surrounding regions. For example, GPX4, GSTP1, MGST3, SOD1, and CYB5R3 appear to be heterogeneously expressed despite the annotated cell type. Heterogeneous CYP4Z1 expression was observed mainly in tumor regions, but this is likely because it was specifically higher in sample v2 which lacked any annotation of clearly normal regions.

The most highly expressed pharmacogenes and their observed expression in tumor, tumor-associated stroma, lymphocytes, and normal tissues are shown in Figure 3. Supplementary Figure S3 shows increased heterogeneity in some genes across tumor regions compared to the composite of other (non-tumor) regions.

In addition to heterogeneous expression, we observed statistically significant differences in the overall expression of pharmacogenes in tumor regions compared to adjacent regions. Figure 4A illustrates differential expression of pharmacogenes between tumor regions and adjacent non-tumor regions. We noticed pharmacogenes tend to be downregulated in tumor regions as can be seen in Figure 4B, however there were still many significantly upregulated genes. Figure 4C shows the top 35 most differentially expressed genes, with ADH1B and GPX3 being significantly downregulated in all 6 tissue samples. Figure 4D, 4E, and 4F show subsets of differential expression for ROS genes, ABC transporter genes, and SLC transporter genes, respectively. These subsets generally do not show obvious differences in ROS or transporter gene expression associated with tumor pathology (except, perhaps, for GPX3). Samples a1 and b1 were post-chemotherapy treated and showed significantly upregulated transporters in ABCA4, ABCC6, and ABCC3. This study was not designed to test the effect of treatment on transporter expression-mediated survival and selection, however, so these results need follow up studies for confirmation.

Biological processes altered by top hits

We conducted a GO pathway analysis to identify the GO terms that are significantly overrepresented by the 66 heterogeneously expressed pharmacogenes. The 45 most significant GO terms (Bonferroni-corrected p-value < 0.05) associated with the 66 heterogeneously expressed pharmacogenes are listed in Supplementary Table S3. As expected, we found a predominance of genes involved in reactive oxygen species handling in addition to drug and metabolite transport.

Discussion

We analyzed the spatial expression patterns of pharmacogenes in six human breast tumor samples and found pharmacogene expression to be heterogeneous within tumor regions. We also showed statistically significant differences in expression of pharmacogenes in tumor regions compared to surrounding non-tumor regions. We observed that the most heterogeneously expressed genes were involved in ROS handling and detoxification mechanisms. The heterogeneous expression of these pharmacogenes may have important implications for cancer therapy due to their ability to impact drug distribution and efficacy throughout the tumor.

The Visium Spatial Transcriptomics platform measures the expression of the whole transcriptome within intact fresh-frozen tissue sections while simultaneously preserving the spatial context of gene expression. The technology relies on spatially barcoded poly-T capture probes that hybridize with mRNA. Due to this non-specific mRNA capture mechanism, highly expressed genes may be captured more frequently than genes expressed at relatively lower levels, limiting sensitivity. Among all six tissue specimens, 214 pharmacogenes were detected, albeit many at lower levels compared to the most highly expressed genes. While the relative expression of pharmacogenes across different histologic regions were comparable across all six tissue samples, larger numbers of uniquely barcoded reads were reported in samples with higher sequencing depth. Future development of capture probes specifically designed for pharmacogenes may improve the sensitivity of their detection.

Heterogeneity was defined as the interquartile range of unique-UMI reads measured across each UMI-barcoded pharmacogene for every spatial spot. Gene expression in each spot may not be uniform; for example, spots within stromal tissue sections will have markedly lower gene expression when compared to spots within tumor regions. To account for such variability in gene expression across the entire tissue, we normalized the read counts to the total number of UMIs detected in each spot. We have presented the data both with and without such normalization because the process of normalization may undermine some of the observed heterogeneity in pharmacogenes. For example, overexpression of other cancer-related genes relative to a given pharmacogene in a tumor region may result in a high total UMI count leading to a masking effect caused by normalization.

Our study evaluated spatial heterogeneity in tumor pharmacogene expression but did not evaluate the downstream impact of this heterogeneity. However, the literature supports the hypothesis that spatial heterogeneity in tumor pharmacogene expression contributes to chemotherapeutic resistance mechanisms. For example, certain drug and metabolite transporters, such as those included in the multidrug resistance protein (MRP) group of the large ABC family, are known to play a role in chemoresistance when overexpressed as they contribute to the efflux of chemotherapeutic compounds from the cell (34). One of these transporters, ABCC5, was among our most heterogeneously expressed pharmacogenes. ABCC5 transports cyclic nucleotides, including the metabolites of 5-fluorouracil (5-FU), a common anticancer agent used in both breast cancer and colon cancer treatment. ABCC5-transfected cells have been shown to have a nearly 9-fold increase in 5-FU resistance (34). Another transporter in this same family also found to be heterogeneously expressed is ABCB8; it transports compounds from the mitochondria to the cytosol. One study showed inhibition of ABCB8 with shRNA resulted in increased

doxorubicin-induced mitochondrial DNA damage (35). This evidence for ABCC5 and ABCB8, combined with our detection of spatial heterogeneity in expression of these genes within breast tumors, provides further mechanistic clarity for how 5-FU or doxorubicin treatment could result in seeding resistant tumor cells following chemotherapy.

Several of the pharmacogenes with the highest heterogeneity (e.g. GPX4, GSTP1, MGST3, and SOD1) are also known to impact drug response. Glutathione peroxidases (GPX) are enzymes that protect cells from oxidative stress by catalyzing the reduction of peroxides. GPX4 has been shown to be critical for survival of lapatinib-resistant cancer cells, but not lapatinib-naïve cancer cells (32). In colorectal cancer, increased GPX3 expression resulted in increased resistance to oxaliplatin and cisplatin (36). This evidence, combined with our detection of spatial heterogeneity in GPX3 and GPX4 expression within tumors, could explain why certain cells survive platinum-agent or lapatinib treatment, leading to resistant tumors.

GSTP1 was also highly heterogeneously expressed in our data. Enzymes in the glutathione s-transferase (GST) family catalyze the conjugation of polar glutathione groups that enhance systemic elimination of chemotherapeutic agents and toxic metabolites. GST activity has been shown to be inducible by treatment with vincristine, doxorubicin, or topotecan (37). When GSTP1 enzymatic activity is impaired, as is the case with the rs1695 missense variant (38), platinum-based chemotherapy-induced granulocytopenia was shown to be more common in a meta-analysis of 12 case control trials (39). Additionally, GSTP1 expression was found to be higher in adriamycin-resistant cells, and higher GSTP1 expression was also found in breast cancer tissues from subjects with progressive/stable disease vs. those with partial/complete response. Interestingly, this finding was true for tissue collected before and after anthracycline/taxane treatment, indicating intrinsic mechanisms of resistance. These data indicate that spatial differences in GSTP1 expression could be involved in chemoresistance and seeding of resistant tumor cells following chemotherapy treatment.

MGST3 was another highly heterogeneously expressed gene in our data. This enzyme is involved in immune function by catalyzing the conjugation of reduced glutathione and leukotriene A4, producing leukotriene C4. Overexpression of MGST3 was found in cisplatin resistant lung adenocarcinoma cells compared to non-resistant progenitor cells, and when MGST3 expression was increased (via antagonism with its microRNA regulator, mir-432-5p) the progenitor cells demonstrated increased survival to cisplatin treatment (40). Although it is unclear if this relates to immune modulation, these data and other similar studies (41, 42) indicate that spatial differences in MGST3 expression could be involved in chemoresistance and seeding of resistant tumor cells following chemotherapy treatment.

Another highly heterogeneously expressed gene in our data was superoxide dismutase 1 (SOD1). SOD1 eliminates damaging superoxide radicals by converting them to less toxic molecular oxygen and hydrogen peroxide. SOD activity counteracts superoxide-induced autophagy (43) and inhibition of SOD1 with siRNA or small molecule inhibitors results in increased cisplatin sensitivity in ovarian cancer cells (44, 45). These studies combined with our results suggest spatial differences in SOD1 expression could be involved in chemoresistance and seeding of resistant tumor cells following chemotherapy treatment.

We acknowledge some limitations to our study. First, we have a small sample size and more information will likely be gained from bigger studies. Second, the lower expressed genes may contain additional variability due to the low read numbers. Third, the resolution is not small enough to capture single cell resolution, so there may be some overlap in cell types.

Conclusions

Our data show substantial heterogeneity in the expression of many pharmacogenes across areas of the breast tumors. These results provide more quantitative expression measurements across spatial regions of tumors. Our results provide more detail on the current understanding of chemoresistance development by providing evidence that there is heterogeneity in the expression of these chemoresistance genes across tumor sub-regions. Notably, our results suggest that chemoresistance caused by GPX4, GSTP1, MGST3, and SOD1 may be intrinsic, not acquired, since the heterogeneity is not specific to chemotherapy-treated samples or cell type. Additionally, we demonstrate the utility of spatial transcriptomics to identify chemo-resistant regions of cells within a tumor and this technology should enable further studies aiming to understand how to overcome this mechanism of resistance.

Declarations

Ethics approval and consent to participate:

Tissues were obtained from the Indiana Biobank under the approved IRB protocol (number 1803676586) at Indiana University.

Consent for publication:

Consent for research and publication of de-identified research information was provided by subjects of the Indiana Biobank.

Availability of data and materials:

Data files are available upon reasonable request from the corresponding author.

Competing interests:

Joseph Ipe began working at 10x Genomics after this study was completed, and while no conflict of interest existed during the study, this statement is provided for full disclosure. None of the other authors have potential conflicts of interest related to this work.

Funding:

This work was supported by NIH-NIGMS grants: T32GM008425 (NRP), and T32GM842528 (RMS), the Vera Bradley Foundation for Breast Cancer Research (JI), and the Indiana University Grand Challenge Precision Health Initiative (JI).

Author Contributions:

NRP wrote manuscript, designed research, and performed analysis.

RMS wrote manuscript, designed research, and performed analysis.

JSH wrote manuscript and designed research.

SB designed research and performed analysis.

TCS wrote manuscript and designed research.

JI wrote manuscript, designed research, and performed experiments.

Acknowledgements:

Sequencing analysis was carried out in the Center for Medical Genomics at Indiana University School of Medicine. Biospecimens were stored in the Clinical and Translational Sciences Institute (CTSI) Specimen Storage Facility which is supported, in part, by grant NIH/NCRR RR020128. Biospecimens were obtained with support from the Indiana CTSI funded, in part by Award Number UL1TR002529 from the National Institutes of Health, National Center for Advancing Translational Sciences, Clinical and Translational Sciences Award. The content is solely the responsibility of the authors and does not necessarily represent the official views of the National Institutes of Health.

References

1. Guo M, Peng Y, Gao A, Du C, Herman JG. Epigenetic heterogeneity in cancer. Biomark Res 2019;7:23
2. Ghosh D, Nandi S, Bhattacharjee S. Combination therapy to checkmate Glioblastoma: clinical challenges and advances. Clin Transl Med 2018;7:33
3. Zhuo JY, Lu D, Tan WY, Zheng SS, Shen YQ, Xu X. CK19-positive Hepatocellular Carcinoma is a Characteristic Subtype. J Cancer 2020;11:5069–77
4. Scherber RM, Mesa RA. Management of challenging myelofibrosis after JAK inhibitor failure and/or progression. Blood Rev 2020;42:100716
5. Vitale I, Shema E, Loi S, Galluzzi L. Intratumoral heterogeneity in cancer progression and response to immunotherapy. Nat Med 2021;27:212–24

6. Beca F, Polyak K. Intratumor Heterogeneity in Breast Cancer. Adv Exp Med Biol 2016;882:169–89
7. Ng CK, Pemberton HN, Reis-Filho JS. Breast cancer intratumor genetic heterogeneity: causes and implications. Expert Rev Anticancer Ther 2012;12:1021–32
8. Katoh M. Canonical and non-canonical WNT signaling in cancer stem cells and their niches: Cellular heterogeneity, omics reprogramming, targeted therapy and tumor plasticity (Review). Int J Oncol 2017;51:1357–69
9. Annaratone L, Simonetti M, Wernersson E, Marchiò C, Garnerone S, Scalzo MS, *et al.* Quantification of HER2 and estrogen receptor heterogeneity in breast cancer by single-molecule RNA fluorescence in situ hybridization. Oncotarget 2017;8:18680–98
10. Grosselin K, Durand A, Marsolier J, Poitou A, Marangoni E, Nemati F, *et al.* High-throughput single-cell ChIP-seq identifies heterogeneity of chromatin states in breast cancer. Nat Genet 2019;51:1060–6
11. Wang Y, Kartasalo K, Weitz P, Acs B, Valkonen M, Larsson C, *et al.* Predicting molecular phenotypes from histopathology images: a transcriptome-wide expression-morphology analysis in breast cancer. Cancer Res 2021
12. Puram SV, Tirosh I, Parikh AS, Patel AP, Yizhak K, Gillespie S, *et al.* Single-Cell Transcriptomic Analysis of Primary and Metastatic Tumor Ecosystems in Head and Neck Cancer. Cell 2017;171:1611-24.e24
13. Xu T, Stewart KM, Wang X, Liu K, Xie M, Ryu JK, *et al.* Metabolic control of T(H)17 and induced T(reg) cell balance by an epigenetic mechanism. Nature 2017;548:228–33
14. Yuan X, Wang J, Huang Y, Shangguan D, Zhang P. Single-Cell Profiling to Explore Immunological Heterogeneity of Tumor Microenvironment in Breast Cancer. Front Immunol 2021;12:643692
15. Dewhirst MW, Cao Y, Moeller B. Cycling hypoxia and free radicals regulate angiogenesis and radiotherapy response. Nat Rev Cancer 2008;8:425–37
16. Michiels C, Tellier C, Feron O. Cycling hypoxia: A key feature of the tumor microenvironment. Biochim Biophys Acta 2016;1866:76–86
17. Parkash J, Felty Q, Roy D. Estrogen exerts a spatial and temporal influence on reactive oxygen species generation that precedes calcium uptake in high-capacity mitochondria: implications for rapid nongenomic signaling of cell growth. Biochemistry 2006;45:2872–81
18. Wang Y, Ma S, Ruzzo WL. Spatial modeling of prostate cancer metabolic gene expression reveals extensive heterogeneity and selective vulnerabilities. Sci Rep 2020;10:3490
19. Roider T, Seufert J, Uvarovskii A, Frauhammer F, Bordas M, Abedpour N, *et al.* Dissecting intratumour heterogeneity of nodal B-cell lymphomas at the transcriptional, genetic and drug-response levels. Nat Cell Biol 2020;22:896–906
20. Fuso Nerini I, Morosi L, Zucchetti M, Ballerini A, Giavazzi R, D'Incalci M. Intratumor heterogeneity and its impact on drug distribution and sensitivity. Clin Pharmacol Ther 2014;96:224–38
21. Fu F, Nowak MA, Bonhoeffer S. Spatial heterogeneity in drug concentrations can facilitate the emergence of resistance to cancer therapy. PLoS Comput Biol 2015;11:e1004142

22. Wang Y, Wang Y, Qin Z, Cai S, Yu L, Hu H, *et al.* The role of non-coding RNAs in ABC transporters regulation and their clinical implications of multidrug resistance in cancer. Expert Opin Drug Metab Toxicol 2021;17:291–306
23. Choi YH, Yu AM. ABC transporters in multidrug resistance and pharmacokinetics, and strategies for drug development. Curr Pharm Des 2014;20:793–807
24. Gillet JP, Gottesman MM. Mechanisms of multidrug resistance in cancer. Methods Mol Biol 2010;596:47–76
25. Assaraf YG, Brozovic A, Gonçalves AC, Jurkovicova D, Linē A, Machuqueiro M, *et al.* The multi-factorial nature of clinical multidrug resistance in cancer. Drug Resist Updat 2019;46:100645
26. Li W, Zhang H, Assaraf YG, Zhao K, Xu X, Xie J, *et al.* Overcoming ABC transporter-mediated multidrug resistance: Molecular mechanisms and novel therapeutic drug strategies. Drug Resist Updat 2016;27:14–29
27. Wu ZX, Teng QX, Cai CY, Wang JQ, Lei ZN, Yang Y, *et al.* Tepotinib reverses ABCB1-mediated multidrug resistance in cancer cells. Biochem Pharmacol 2019;166:120–7
28. Baron M, Tagore M, Hunter MV, Kim IS, Moncada R, Yan Y, *et al.* The Stress-Like Cancer Cell State Is a Consistent Component of Tumorigenesis. Cell Syst 2020;11:536-46.e7
29. Ryoo IG, Lee SH, Kwak MK. Redox Modulating NRF2: A Potential Mediator of Cancer Stem Cell Resistance. Oxid Med Cell Longev 2016;2016:2428153
30. Kim B, Jung JW, Jung J, Han Y, Suh DH, Kim HS, *et al.* PGC1α induced by reactive oxygen species contributes to chemoresistance of ovarian cancer cells. Oncotarget 2017;8:60299–311
31. Griess B, Mir S, Datta K, Teoh-Fitzgerald M. Scavenging reactive oxygen species selectively inhibits M2 macrophage polarization and their pro-tumorigenic function in part, via Stat3 suppression. Free Radic Biol Med 2020;147:48–60
32. Hangauer MJ, Viswanathan VS, Ryan MJ, Bole D, Eaton JK, Matov A, *et al.* Drug-tolerant persister cancer cells are vulnerable to GPX4 inhibition. Nature 2017;551:247–50
33. Ståhl PL, Salmén F, Vickovic S, Lundmark A, Navarro JF, Magnusson J, *et al.* Visualization and analysis of gene expression in tissue sections by spatial transcriptomics. Science 2016;353:78–82
34. Pratt S, Shepard RL, Kandasamy RA, Johnston PA, Perry W, 3rd, Dantzig AH. The multidrug resistance protein 5 (ABCC5) confers resistance to 5-fluorouracil and transports its monophosphorylated metabolites. Mol Cancer Ther 2005;4:855–63
35. Elliott AM, Al-Hajj MA. ABCB8 mediates doxorubicin resistance in melanoma cells by protecting the mitochondrial genome. Mol Cancer Res 2009;7:79–87
36. Pelosof L, Yerram S, Armstrong T, Chu N, Danilova L, Yanagisawa B, *et al.* GPX3 promoter methylation predicts platinum sensitivity in colorectal cancer. Epigenetics 2017;12:540–50
37. Seitz G, Bonin M, Fuchs J, Poths S, Ruck P, Warmann SW, *et al.* Inhibition of glutathione-S-transferase as a treatment strategy for multidrug resistance in childhood rhabdomyosarcoma. Int J Oncol 2010;36:491–500

38. Watson MA, Stewart RK, Smith GB, Massey TE, Bell DA. Human glutathione S-transferase P1 polymorphisms: relationship to lung tissue enzyme activity and population frequency distribution. Carcinogenesis 1998;19:275–80
39. Lv F, Ma Y, Zhang Y, Li Z. Relationship between GSTP1 rs1695 gene polymorphism and myelosuppression induced by platinum-based drugs: a meta-analysis. Int J Biol Markers 2018;33:364–71
40. Zhang J, Xu C, Gao Y, Wang Y, Ding Z, Zhang Y, *et al.* A Novel Long Non-coding RNA, MSTRG.51053.2 Regulates Cisplatin Resistance by Sponging the miR-432-5p in Non-small Cell Lung Cancer Cells. Front Oncol 2020;10:215
41. Matulis SM, Morales AA, Yehiayan L, Lee KP, Cai Y, Boise LH. Alterations in glutathione levels and apoptotic regulators are associated with acquisition of arsenic trioxide resistance in multiple myeloma. PLoS One 2012;7:e52662
42. Efferth T, Volm M. Glutathione-related enzymes contribute to resistance of tumor cells and low toxicity in normal organs to artesunate. In Vivo 2005;19:225–32
43. Chen Y, Azad MB, Gibson SB. Superoxide is the major reactive oxygen species regulating autophagy. Cell Death Differ 2009;16:1040–52
44. Brown DP, Chin-Sinex H, Nie B, Mendonca MS, Wang M. Targeting superoxide dismutase 1 to overcome cisplatin resistance in human ovarian cancer. Cancer Chemother Pharmacol 2009;63:723–30
45. Kim JW, Sahm H, You J, Wang M. Knock-down of superoxide dismutase 1 sensitizes cisplatin-resistant human ovarian cancer cells. Anticancer Res 2010;30:2577–81

Figures

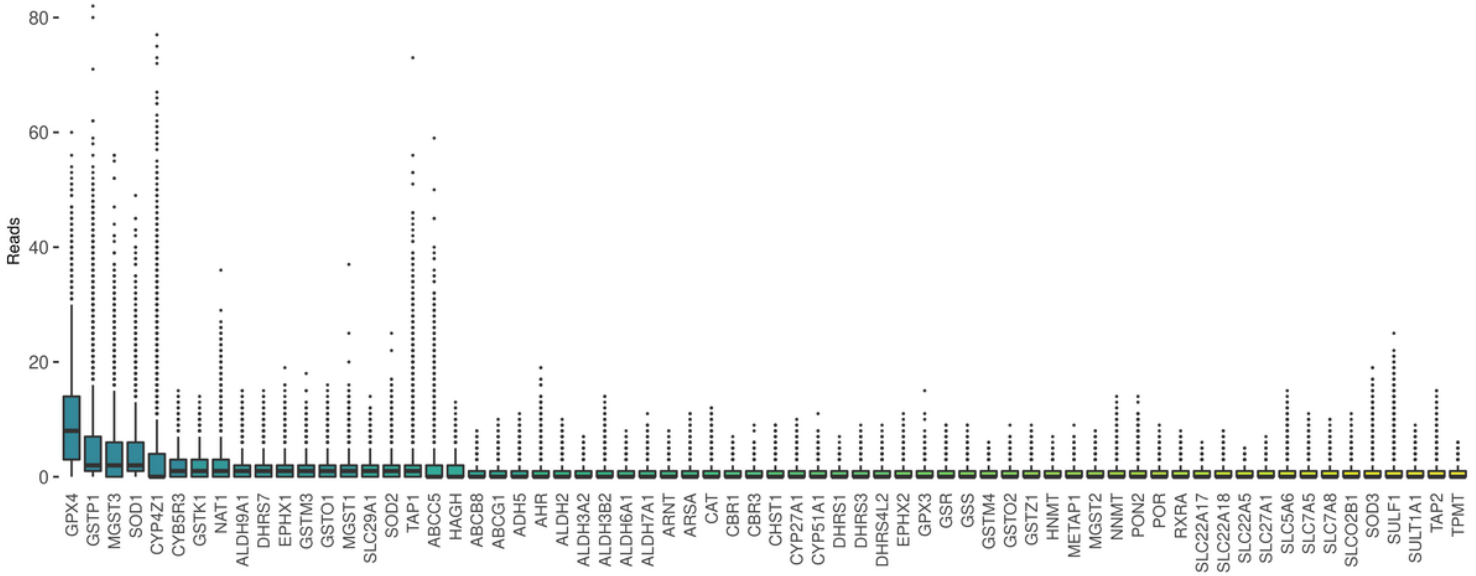

Figure 1

Boxplot of all pharmacogenes, across all samples, in tumor regions only, with an interquartile range greater than zero. Each data point on the y-axis is the number of unique-UMI reads from a single barcoded dot. The genes on the X-axis are sorted by interquartile range in descending order.

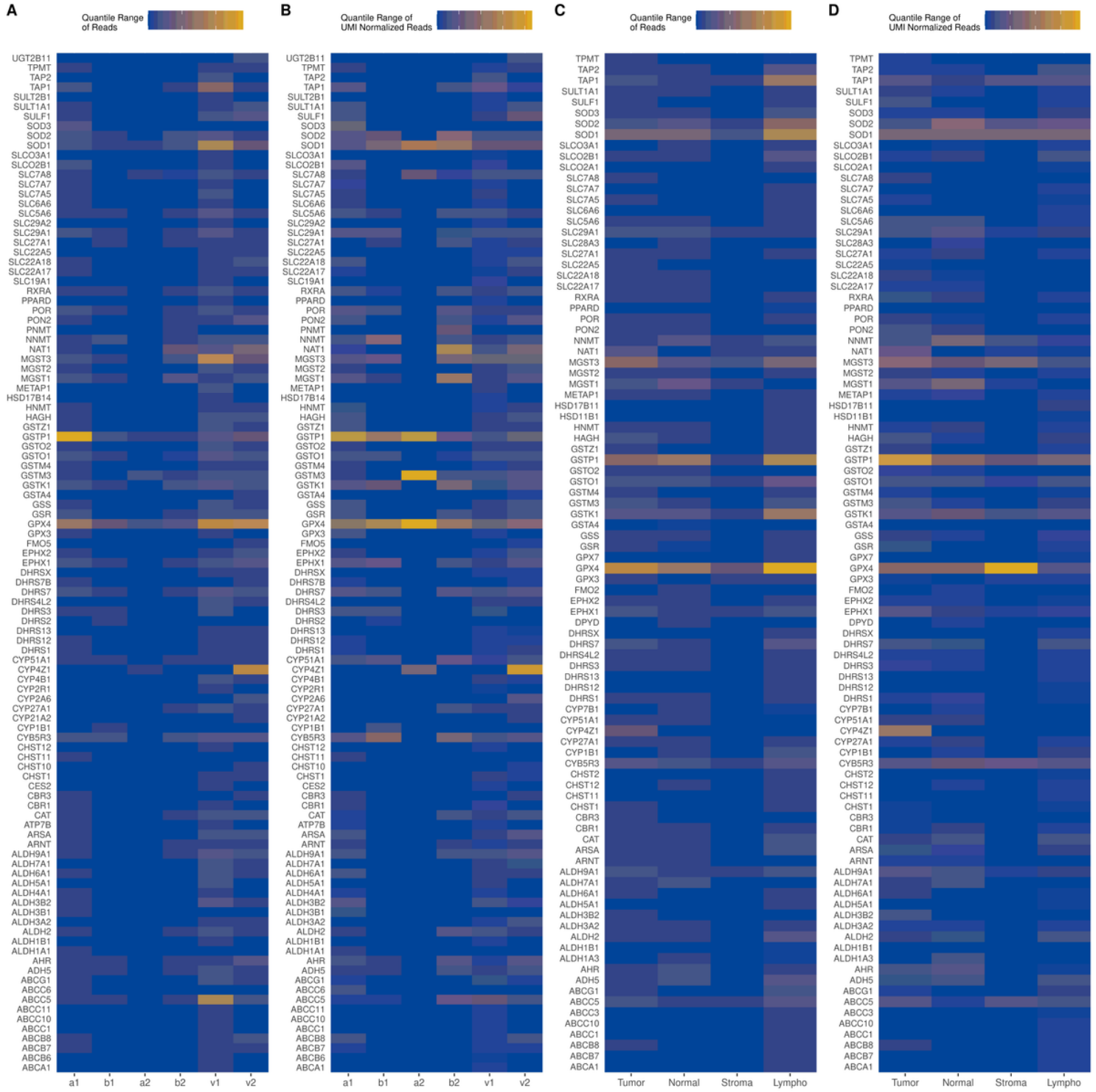

Figure 2

Intensity maps showing subsets of pharmacogenes with an interquartile range greater than 0 in any of the groups on the x-axis. (A) Interquartile range of unique-UMI reads for each gene for each sample in tumor spots. (B) Interquartile range of UMI-normalized unique-UMI reads for each gene for each sample in

tumor spots. C) Interquartile range of unique-UMI reads for each gene for each annotated region. D) Interquartile range of UMI-normalized unique-UMI reads for each gene for each annotated region.

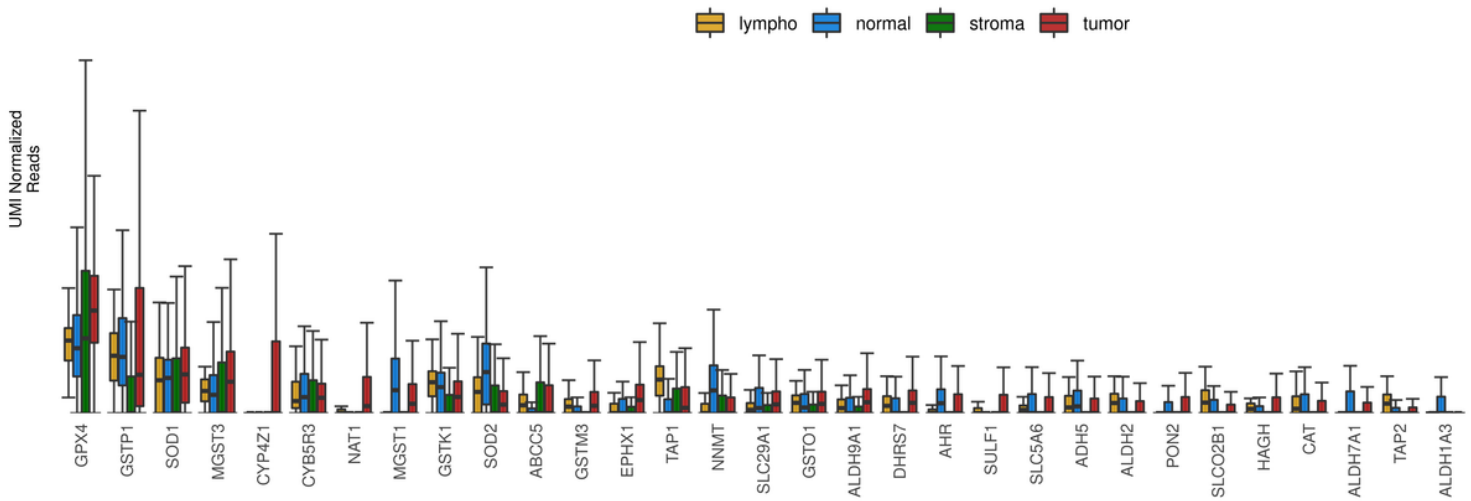

Figure 3

Boxplots of UMI-normalized unique-UMI reads for subsets of pharmacogenes with the top 31 largest interquartile ranges. Groups are divided into tumor (tumor + DCIS + cellular tumor + desmoplastic tumor), normal, lymphocytes, and stroma. Y-axis scale is arbitrary, as this figure is intended to show relative differences.

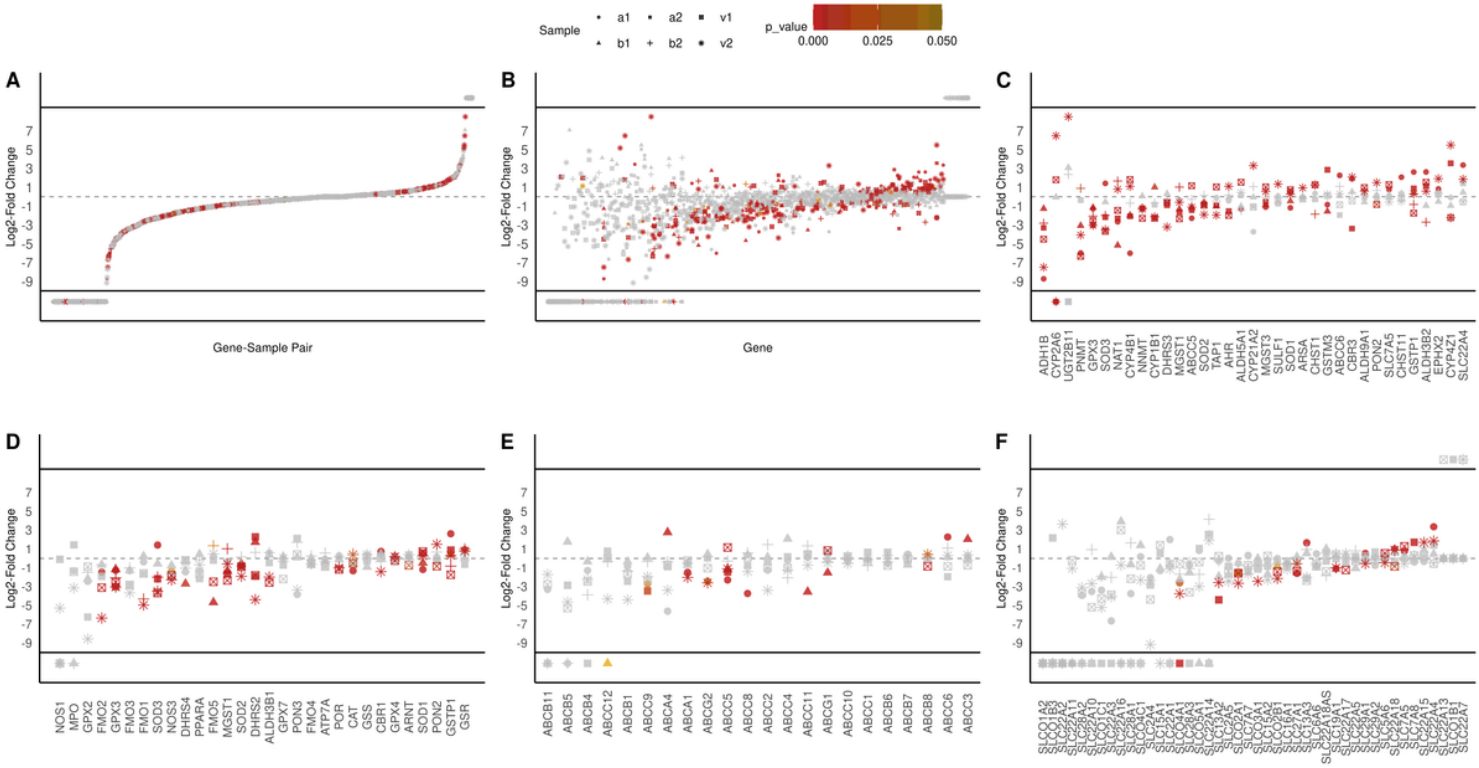

Figure 4

Log2 fold change comparisons for UMI-normalized unique-UMI reads, for tumor regions (per sample) vs. combined non-tumor regions across all samples. The X-axis is in ascending order by average fold change per group. P-values are based two-sided Welch's t-tests, are Bonferroni corrected, and are colored by intensity. Shapes denote which sample the fold change is based on. Values above and below the black bars represent divide-by-zero values of infinity or negative infinity; these values were kept because one of the groups in the comparison had an average of zero expression while the other group had non-zero expression, indicating a potentially significant differential expression. A) S-plot showing the distribution for each gene-sample combination. B) Global comparison by pharmacogene. C) Subset of 35 genes with the lowest p-values. D) Subset of genes involved in reactive oxygen species handling. E) ABC transporter subset. F) SLC transporters subset.

Supplementary Files

This is a list of supplementary files associated with this preprint. Click to download.

- SupplementalFigures.docx
- SupplementalTables.docx